Landau Quantization and the Thickness Limit of Topological Insulator Thin Films of Sb_2Te_3

Yeping Jiang,[1,2] Yilin Wang,[1] Mu Chen,[1,2] Zhi Li,[1] Canli Song,[1,2] Ke He,[1] Lili Wang,[1] Xi Chen,[2] Xucun Ma,[1,*] and Qi-Kun Xue[1,2,†]

[1]*Institute of Physics, Chinese Academy of Sciences, Beijing 100190, People's Republic of China*
[2]*State Key Laboratory of Low-Dimensional Quantum Physics, Department of Physics, Tsinghua University, Beijing 100084, People's Republic of China*
(Received 16 August 2011; published 3 January 2012)

We report the experimental observation of Landau quantization of molecular beam epitaxy grown Sb_2Te_3 thin films by a low-temperature scanning tunneling microscope. Different from all the reported systems, the Landau quantization in a Sb_2Te_3 topological insulator is not sensitive to the intrinsic substitutional defects in the films. As a result, a nearly perfect linear energy dispersion of surface states as a 2D massless Dirac fermion system is achieved. We demonstrate that four quintuple layers are the thickness limit for a Sb_2Te_3 thin film being a 3D topological insulator. The mechanism of the Landau-level broadening is discussed in terms of enhanced quasiparticle lifetime.

DOI: 10.1103/PhysRevLett.108.016401 PACS numbers: 71.70.Di, 68.37.Ef, 72.25.−b, 73.20.−r

A topological insulator (TI) [1,2] is characterized by nontrivial gapless states on its surface or boundary due to strong spin-orbit coupling [3]. The surface states (SS) of a strong TI are massless Dirac fermions (DFs) and consist of an odd number of Dirac cones, centering at the time-reversal invariant momentums that are robust against any time-reversal invariant perturbation [4]. Recently, a class of strong TIs (Bi_2Te_3, Bi_2Se_3, and Sb_2Te_3) with a relatively large bulk energy gap and a single SS Dirac cone has been theoretically predicted [5] and experimentally proved [6–8]. The helical SS lead to a nonzero Berry's phase (π) of the electron wave function and a series of exotic phenomena such as the absence of backscattering [9–12] and weak antilocalization [13]. In the case of thin films, at a critical thickness the SS from opposite surfaces of the films can couple together and open a thickness-dependent gap [14–16], which is nontrivial and may give rise to a quantum spin Hall state similar to the case of HgTe quantum wells [17].

Despite recent extensive reports on TIs, the experimental study on Sb_2Te_3 is unexpectedly rare [8,18]. The main reason is the material. Because of the relatively weak bonding between Sb and Te and the molecular nature of both Sb and Te beams, Sb vacancies and antisite (Sb_{Te}) defects can easily form. Thus, as-grown Sb_2Te_3 is heavily p doped with its Fermi level (E_F) lying in the bulk valence band. As shown in this study, the situation can be changed by growing high quality crystalline Sb_2Te_3 films by molecular beam epitaxy (MBE). The high quality films grown by MBE allow us to investigate topological SS and the effect of those intrinsic defects directly by *in situ* scanning tunneling microscopy (STM) and scanning tunneling spectroscopy (STS). In spite of a large number of intrinsic substitutional defects, our STS measurements reveal well-defined Landau quantization in Sb_2Te_3 films, from which a nearly ideal linear dispersion of SS can be deduced. By studying the thickness dependence of SS, we find that the thickness limit for Sb_2Te_3 being a 3D TI is four quintuple layers (QL). Below 4 QL, an energy gap and its thickness dependence that results from the interaction of SS from the opposite sides of the film are observed.

Our experiments were carried out in a combined ultrahigh vacuum MBE-STM system (Unisoku) with a base pressure of less than 1×10^{-10} Torr. In the MBE growth of Sb_2Te_3 films, highly n-doped 6H-SiC(0001) covered mainly by bilayer graphene was used as the substrate [19]. The inert graphene avoids interface chemical reaction and leads to an atomically sharp interface [19], which is crucial for the current study. Sb_2Te_3 films were prepared by thermal evaporation of high-purity Sb (99.9999%) and Te (99.9999%) from two standard Knudsen cells. The temperatures of the Sb source, the Te source, and the substrate were set at 330 °C, 225 °C, and 230 °C, respectively, which results in a growth rate of ~0.2 QL/min. While the defects in Bi_2Te_3 can be n- or p-type by different growth conditions [20] and in Bi_2Se_3 can only be n-type [19], two types of intrinsic defects, Sb vacancy and Sb_{Te} antisite defect, are all proved to be p-type in Sb_2Te_3 [21]. The defect formation is very sensitive to the effective Sb/Te flux ratio, which can be tuned by changing the substrate temperature because of the temperature dependent sticking coefficient of Sb and Te on the surface. The latter defect appears at relatively higher substrate temperatures, while the former dominates at lower temperatures (both can be minimized by fine-tuning of growth conditions) [21]. In this work, three kinds of samples (type-I, -II, and -III) were investigated. Type-I (~ 30 QL thick, Fig. 1) samples were prepared at medium substrate temperature (~ 230 °C). Type-II samples (3–8 QL thick, Fig. 2) contain more substitutional defects, which were prepared by annealing type-I samples at ~250 °C. Type-III samples (1–8 QL, Fig. 3) were grown at relatively low

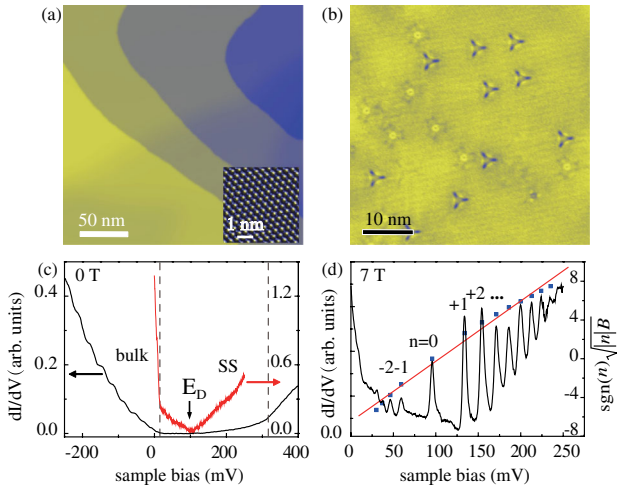

FIG. 1 (color online). (a) STM topographic image of 30 QL type-I sample prepared by MBE. Tunneling conditions are $V_{\mathrm{bias}} = 5.0$ V, $I = 50$ pA. The bias voltage is applied to the sample. The inset shows an atomic resolution image of Sb_2Te_3 (111) surface (20 mV, 0.1 nA). The brighter spots correspond to Te atoms. (b) STM topographic image (1.0 V, 50 pA) showing the typical surface defects of the sample. (c) Bulk (setpoint: $V_{\mathrm{bias}} = 0.3$ V, $I = 50$ pA) and SS spectra (0.25 V, 0.2 nA) in the energy gap. Because of the much lower SS DOS compared with bulk DOS, a much closer tunneling gap is needed to reveal the detail of SS. (d) Landau quantization of topological SS at 7 T (curve), relation between LL energies and $\mathrm{sgn}(n)\sqrt{|n|B}$ (squares), and a linear fitting to the relation (line). The bias modulation was 1 mV at 987.5 Hz.

temperature ($\sim 200\,^{\circ}$C). In this case, the dominating defects are Sb vacancies.

The morphology of the type-I sample is shown in Fig. 1(a), in which wide terraces separated by regular steps with a height of about 1.01 nm can be seen. The inset in Fig. 1(a) shows the atomic resolution image of the surface. The surface is a Te-terminated (111) surface with a lattice constant of about 4.26 Å. High-density ($\sim 10^{12}$ cm^{-2}) clover-shaped defects can be clearly seen in Fig. 1(b). They are Sb_{Te1} and Sb_{Te3} in the first QL, as identified by atomic resolution images [21]. Here Te1 and Te3 correspond to the first-layer and third-layer Te atoms from the surface.

The dI/dV spectrum in STM measures the local density of states (LDOS) of a sample surface at various energies. In Fig. 1(c), we show dI/dV spectrum of a type-I sample from -250 meV to $+400$ meV at zero magnetic field. The sharp increase in LDOS around 0 meV (E_F) and above 300 meV indicates a bulk energy gap of $\sim$300 meV, where the energy of about 15 meV above E_F can be attributed to the bulk valence band (VB) edge. In the bulk gap, a typical V-shaped spectrum with a conductance minimum representing the Dirac point (DP) at 100 meV above E_F is seen, which is also supported by the occurrence of the zeroth Landau level at this energy in the magnetic field [Fig. 1(d)].

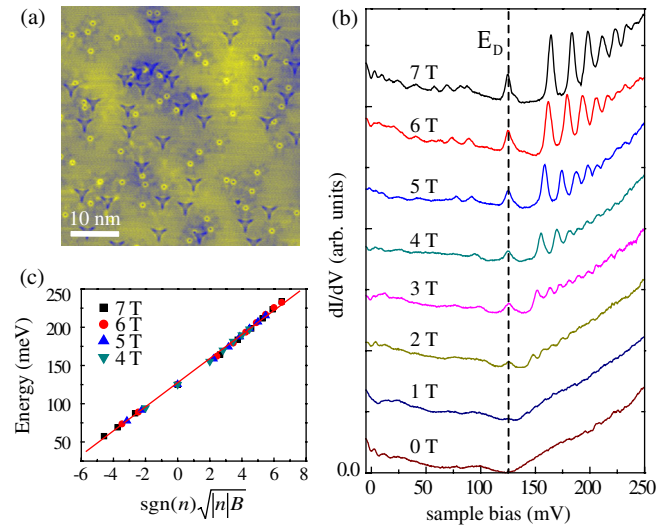

FIG. 2 (color online). (a) STM topographic image (1.0 V, 50 pA) showing the surface defects of 7 QL type-II sample. (b) dI/dV spectra (0.25 V, 0.2 nA) from 0 to 7 T. The dotted line indicates a field-independent $n = 0$ LL at the Dirac point. Spectra under different fields are shifted vertically for clarity. (c) LL energies under various magnetic fields plotted versus $\mathrm{sgn}(n)\sqrt{|n|B}$. The line is a linear fitting to the data.

The nearly zero tunneling conductance at the DP and the V-shaped LDOS are consistent with the Dirac cone structure of the SS. Therefore, we know that the DP in the 30 QL Sb_2Te_3 film is separated from the bulk VB edge by 85 meV.

The 2D massless DF nature of the SS can be revealed by Landau-level (LL) spectroscopy [22,23]. In the presence of a perpendicular magnetic field, the momentum and energy of SS electrons are quantized into discrete values, E_n and $k_n = \sqrt{2e|n|B/\hbar}$, $n = 0, \pm 1, \pm 2, \ldots$ [23], where e is the elementary charge, n is the LL index, B is the magnetic field, and $\hbar$ is the reduced Plank constant. The values of E_n are determined by Lorenzian fits of peaks in the LL spectra. The LL spectrum of massless DFs follows the unique square root dependent sequence,

$$E_n = E_D + \mathrm{sgn}(n)\nu_F\sqrt{2e\hbar|n|B}, \qquad n = 0, \pm 1, \pm 2, \ldots, \tag{1}$$

where ν_F is the Fermi velocity and E_D is the DP energy.

Figure 1(d) shows the LL spectrum of the type-I sample at a magnetic field of 7 T (curve). A series of nonequally spaced sharp LL peaks can be observed. One of the unique features of the LL sequence is the appearance of a peak at the DP where the LDOS is basically zero in the zero-field spectrum [Fig. 1(c)]. This LL_0 peak is independent of B [Figs. 2(b) and 4(a)]. It is an indication of the chiral nature of Sb_2Te_3 SS, which is closely related to the nontrivial Berry's phase [24]. Below the zero mode, at least two peaks can be explicitly resolved, though the intensity is suppressed probably due to a coupling to the VB states. The DP of Sb_2Te_3 SS is well above its VB, which is in

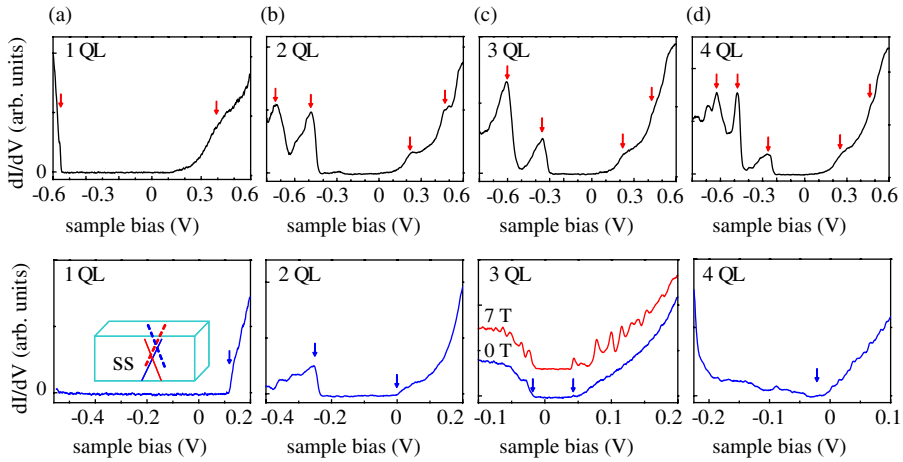

FIG. 3 (color online). (a)–(d) dI/dV spectra of 1–4 QL type-III Sb_2Te_3 films. The bulk QWS are indicated by arrows. The corresponding SS spectrum for each thickness is displayed in the lower panel. The inset in (a) represents two sets of SS on the opposite surfaces. For 3 QL films, the SS spectrum at 7 T is also presented together with zero-field spectrum in the lower panel of (c), which were taken on type-II samples for better quality [35].

sharp contrast to Bi_2Te_3 with the DP buried in the VB [6] and to Bi_2Se_3 with the DP in close proximity to the VB [7,22,23]. We plot the LL energies E_n at 7 T versus $\mathrm{sgn}(n)\sqrt{|n|}$ in Fig. 1(d) (squares). The dispersion deviates from linearity and is a convex function at the DP, implying a nonzero mass of the SS electrons even at the DP. This is inconsistent with the massless DF nature of topological SS near the DP. We attribute it to the tip-gating effect [22], which is prominent when E_F lies inside the bulk gap and close to the DP.

The tip effect can be eliminated in highly doped and thinner Sb_2Te_3 films. The type-II sample was prepared for this purpose: its surface defect density is approximately 4 times that of the type-I sample [Fig. 2(a)]. Moreover, in a-few-QL samples like type-II, the substrate and highly doped film offer a better screening to the tip's electric field and minimize the tip-induced band bending. Figure 2(b) displays the LL spectra series of a type-II sample at different magnetic fields, where the LLs become notable at 2 T. The field-independent DP is located at ~126 meV above E_F, implying a higher doping level. The LL energies E_n at different B are plotted against $\mathrm{sgn}(n)\sqrt{|n|B}$ related to the quantized momentum in Fig. 2(c). A nearly perfect linearity characteristic of the 2D massless DFs is immediately evident. The resulting Fermi velocity ν_F is 4.3×10^5 ms^{-1}. The observation indicates that the nonlinearity in Fig. 1(d) is not intrinsic.

We then investigate the thickness dependence of the SS. For a TI film below a critical thickness, the coupling between the top and bottom SS with a finite decay length will open an energy gap. For Bi_2Se_3, the critical thickness as determined by angle-resolved photoemission spectroscopy is 6 QL [16]. Here, similar 3D-2D crossover phenomenon was also observed. The type-III sample was used because terraces with a thickness of 1–2 QL only appear at relatively low temperature of the graphene substrate.

Figures 3(a)–3(d) show evolution of bulk quantum well states (QWS) and SS with a film thickness from 1 to 4 QL. The bulk gap determined by the lowest conduction band and highest VB QWS decreases with the increasing thickness. In the gap, there is clear evidence that the SS opens a new and smaller gap below 4 QL. This gap is about 255 meV at 2 QL and decreases to 60 meV at 3 QL. At 1 QL, the lower SS branch is absent, with the sharp increase in LDOS at −550 meV ascribed to the bulk VB edge, which is consistent with theoretic calculations [8]. The gap at 3 QL is manifested with the absence of the zeroth LL in the spectrum at 7 T, where LLs in both of the upper and lower SS branches can be seen [Fig. 3(c)]. At 4 QL, the SS gap nearly vanishes, with the zero-conductance point at −15 meV (see also Fig. S1 in the Supplemental Material [25]).

The conductance minimum in LDOS at 4 QL in Fig. 3(d) is indeed the DP of SS, as demonstrated by the LL spectroscopy [Fig. 4(a)] of a type-II sample (to avoid tip effect). At 4 QL, similar to 7 QL, the emergence of a field-independent zeroth peak and the good linear fitting in LL peaks [Fig. 4(b)] at various B indicate that 4 QL Sb_2Te_3 film is a 3D TI. The DP at 4 QL is ~82 meV, lower in energy than that at 7 QL because of substrate doping. The Fermi velocity ν_F is $\sim 4.6 \times 10^5$ ms^{-1}, a little larger than that in 7 QL films.

From the highly resolved LL peaks in our experiment, the quasiparticle lifetime τ can be extracted. As shown in Fig. 4(c), the LL peak width shows a minimum at E_F, duplicating the enhanced intensity of LLs around zero energy [Fig. 4(a)]. At the energy around LL_0, there is another minimum in the peak-width distribution. This phenomenon might be correlated with three possible scattering channels: electron-electron interaction (EEI), disorder, and electron-phonon coupling. In our case, electron-phonon coupling can be excluded as the main

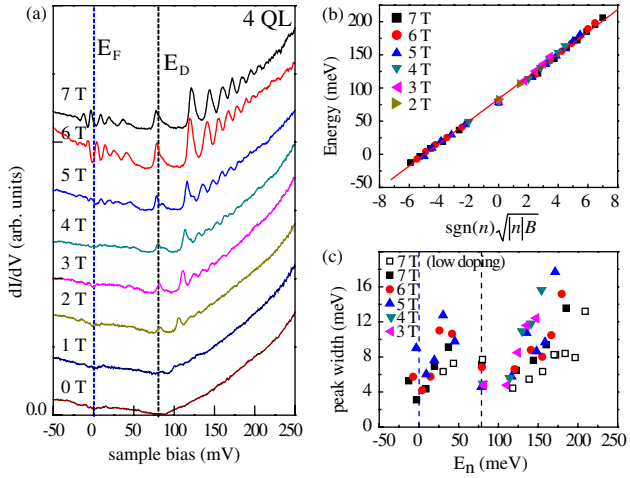

FIG. 4 (color online). (a) dI/dV spectra (0.2 V, $I = 0.2$ nA) of a 4 QL type-II sample from 0 to 7 T. (b) The fitting of the LL energies versus $\mathrm{sgn}(n)\sqrt{|n|B}$ for magnetic fields from 2 to 7 T. (c) Full width at half maximum of LL peaks at different energies in (a) and Fig. 1(d) fitted by Lorentzian function. The hollow squares correspond to the LL peaks in type-I sample in Fig. 1(d) and have been shifted by the energy difference between the DPs of the two different samples.

factor of LL width broadening because it will only lead to an increase in the LL width above certain phonon energy, above which the distribution curve is flat.

Disorder in our atomically flat films mainly comes from the intrinsic substitutional defects (Sb_{Te}), which can also be ruled out for the following two reasons. First, disorder will broaden the LL peaks around E_F [26] and narrow them at energies away from E_F, which is contrary to our observation. Second, the similar peak width of type-I and II samples [Fig. 4(c)] strongly suggests that disorder has little effect. Therefore, Sb_{Te} induced disorder does not have much effect on τ. It is understandable because disorder or impurity may only induce intraband (between SS) scattering when the quasiparticle energy lies well within the bulk gap in our case. In topological insulators, the intraband scattering channel is limited by the helical nature of SS, provided that the Fermi surface is not warped [27]. The quasiparticle has a large probability of not being scattered. Thus this observation can be a testimony of topological surface states' helical nature.

We attribute this unusual peak-width distribution to intraband EEI. Interband EEI (between SS and bulk state electrons) is excluded because of the relatively large bulk gap in our case (injected electron energy is too small to generate electron-hole pair in the bulk). The decay rate of an injected electron through this process increases with energy away from E_F. The enhanced τ at low energies has been observed and ascribed to EEI in graphene [28,29] and Bi_2Se_3 [23]. However, this monotonic trend of scattering rate with respect to energy is modified by the Dirac cone shape of SS. The electron injected into the SS just above the Dirac energy has few relaxation channels that satisfy conservation rules, similar to that in graphene [30] which also has an energy band of Dirac cone shape. This leads to an enhanced τ at energies around the DP. Thus EEI and the Dirac cone together account quite well for the LL peak-width distribution and is suggested as the main relaxation channel for quasiparticles in Sb_2Te_3 thin films. EEI may be increased further in the presence of a magnetic field. Recently, transport measurement on Bi_2Se_3 films suggests the essential role played by EEI in the transport of topological insulators [31,32].

The peak-width value of about 4 meV at two minimums leads to $\tau \sim 0.2$ ps, yielding a mean free path of about 80 nm. This value is comparable to the terrace size in our Sb_2Te_3 films, suggesting that the step edge can act as the scattering source and give the upper limit of the mean free path in Sb_2Te_3 films. Recent work also supports that the in-gap bound states could be induced by the step edge [33]. Compared to the strong impurity induced in-gap resonances [34], Sb_{Te} defects in our films can be defined as "weak" impurities that will not violate the topological protection of SS.

In summary, we have studied the topological SS of Sb_2Te_3 MBE thin films using LL spectroscopy. The exotic property of TI SS in Sb_2Te_3 is demonstrated by revealing the linear dispersion of SS and the field-independent zeroth LL at the DP. The DP in Sb_2Te_3 is found to be well separated from the bulk states. By analyzing the LL peak-width distribution, we found that it is not impurity induced disorder but EEI that limits the quasiparticle lifetime in Sb_2Te_3. We further show that the 3D-to-2D crossover of the SS in Sb_2Te_3 occurs at 4 QL.

This work was supported by National Science Foundation and Ministry of Science and Technology of China. All STM topographic images were processed by WSxM software.

*Corresponding author.
xcma@aphy.iphy.ac.cn
†Corresponding author.
qkxue@mail.tsinghua.edu.cn

[1] M. Z. Hasan and C. L. Kane, Rev. Mod. Phys. **82**, 3045 (2010).
[2] X.-L. Qi and S.-C. Zhang, Rev. Mod. Phys. **83**, 1057 (2011).
[3] C. L. Kane and E. J. Mele, Phys. Rev. Lett. **95**, 146802 (2005).
[4] L. Fu and C. L. Kane, Phys. Rev. B **76**, 045302 (2007).
[5] H. J. Zhang *et al.*, Nature Phys. **5**, 438 (2009).
[6] Y. L. Chen *et al.*, Science **325**, 178 (2009).
[7] Y. Xia *et al.*, Nature Phys. **5**, 398 (2009).
[8] G. Wang *et al.*, Nano Res. **3**, 874 (2010).
[9] Z. Alpichshev *et al.*, Phys. Rev. Lett. **104**, 016401 (2010).
[10] P. Roushan *et al.*, Nature (London) **460**, 1106 (2009).
[11] J. Seo *et al.*, Nature (London) **466**, 343 (2010).
[12] T. Zhang *et al.*, Phys. Rev. Lett. **103**, 266803 (2009).

[13] J. Chen *et al.*, Phys. Rev. Lett. **105**, 176602 (2010).
[14] C.-X. Liu *et al.*, Phys. Rev. B **81**, 041307 (2010).
[15] H.-Z. Lu *et al.*, Phys. Rev. B **81**, 115407 (2010).
[16] Y. Zhang *et al.*, Nature Phys. **6**, 584 (2010).
[17] M. Konig *et al.*, J. Phys. Soc. Jpn. **77**, 031007 (2008).
[18] D. Hsieh *et al.*, Phys. Rev. Lett. **103**, 146401 (2009).
[19] C. L. Song *et al.*, Appl. Phys. Lett. **97**, 143118 (2010).
[20] G. Wang *et al.*, Adv. Mater. **23**, 2929 (2011).
[21] Y. P. Jiang *et al.*, arXiv:1111.0817v1.
[22] P. Cheng *et al.*, Phys. Rev. Lett. **105**, 076801 (2010).
[23] T. Hanaguri *et al.*, Phys. Rev. B **82**, 081305 (2010).
[24] Y. Zhang *et al.*, Nature (London) **438**, 201 (2005).
[25] See Supplemental Material at http://link.aps.org/supplemental/10.1103/PhysRevLett.108.016401 for the detailed evolution of QWS and surface states with film thickness.
[26] N. M. R. Peres, F. Guinea, and A. H. Castro Neto, Phys. Rev. B **73**, 125411 (2006).
[27] L. Fu, Phys. Rev. Lett. **103**, 266801 (2009).
[28] G. Li, A. Luican, and E. Y. Andrei, Phys. Rev. Lett. **102**, 176804 (2009).
[29] J. Gonzalez, F. Guinea, and M. A. H. Vozmediano, Phys. Rev. Lett. **77**, 3589 (1996).
[30] A. Bostwick *et al.*, Nature Phys. **3**, 36 (2006).
[31] M. H. Liu *et al.*, Phys. Rev. B **83**, 165440 (2011).
[32] J. Wang *et al.*, Phys. Rev. B **83**, 245438 (2011).
[33] Z. Alpichshev *et al.*, Phys. Rev. B **84**, 041104(R) (2011).
[34] A. M. Black-Schaffer and A. V. Balatsky, arXiv:1110.5149v1.
[35] Sb vacancies degrade the spectrum quality, probably due to vacancy-induced in-gap resonances.